# Structural determination of the sheath-forming polysaccharide of *Sphaerotilus montanus* using thiopeptidoglycan lyase which recognizes the 1,4 linkage between α-D-GalN and β-D-GlcA

Daisuke Kashiwabara[a], Keiko Kondo[b], Ryoji Usami[a], Daisuke Kan[a], Izuru Kawamura[a], Yuta Kawasaki[a], Michio Sato[c], Tadashi Nittami[a], Ichiro Suzuki[a], Masato Katahira[b,d], Minoru Takeda[a]*

[a]*Faculty of Engineering, Yokohama National University, 79-5 Tokiwadai, Hodogaya, Yokohama 240-8501, Japan*

[b]*Institute of Advanced Energy, Kyoto University, Gokasho, Uji, Kyoto 611-0011, Japan*

[c]*School of Agriculture, Meiji University, 1-1-1 Higashimita, Tama, Kawasaki 214-8571, Japan*

[d]*Graduate School of Energy Science, Kyoto University, Gokasho, Uji, Kyoto 611-0011, Japan*

* Corresponding author: Tel. +81 45 339 4268; Fax +81 45 339 4267; E-mail takeda-minoru-bd@ynu.ac.jp

**Abstract**

*Sphaerotilus natans* is a filamentous sheath-forming bacterium commonly found in activated sludge. Its sheath is assembled from a thiolic glycoconjugate called thiopeptidoglycan. *S. montanus* ATCC-BAA-2725 is a sheath-forming member of stream biofilms, and its sheath is morphologically similar to that of *S. natans.* However, it exhibits heat susceptibility, which distinguishes it from the *S. natans* sheath. In this study, chemical composition and solid-state NMR analyses suggest that the *S. montanus* sheath is free of cysteine, indicating that disulfide linkage is not mandatory for sheath formation. The *S. montanus* sheath was successfully solubilized by *N*-acetylation, allowing solution-state NMR analysis to determine the sugar sequence. The sheath was susceptible to thiopeptidoglycan lyase prepared from the thiopeptidoglycan-assimilating bacterium, *Paenibacillus koleovorans*. The reducing ends of the enzymatic digests were labeled with 4-aminobenzoic acid ethyl ester, followed by HPLC. Two derivatives were detected, and their structures were determined. We found that the sheath has no peptides and is assembled as follows: [→4)-β-D-GlcA-(1→4)-β-D-Glc-(1→3)-β-D-GalNAc-(1→4)-α-D-GalNAc-(1→4)-α-D-GalN-(1→]$_n$ (β-D-Glc and α-D-GalNAc are stoichiometrically and substoichiometrically 3-*O*-acetylated, respectively). Thiopeptidoglycan lyase was thus confirmed to cleave the 1,4 linkage between α-D-GalN and β-D-GlcA, regardless of the peptide moiety. Furthermore, vital fluorescent staining of the sheath demonstrated that elongation takes place at the tips, as with the *S. natans* sheath.

*Keywords:* sheath, *Sphaerotilus montanus*, thiopeptidoglycan lyase

## 1. Introduction

The strains of the genus *Sphaerotilus* of the β-*Proteobacteria* class are filamentous aquatic microbes common in activated sludge and eutrophic streams [1]. Excessive growth of filamentous bacteria including *Sphaerotilus* strains in activated sludge, causes poor settlement of activated sludge, referred to as filamentous bulking [2,3]. Because the cells of *Sphaerotilus* strains are unclumped rods, their filamentation is attributed to the formation of a sheath (microtube) that covers a line of cells. To better understand filamentous bulking, the chemical features of the *Sphaerotilus natans* sheath have been extensively studied. In early investigations, the *Sphaerotilus* sheath was considered to be a polysaccharide, protein, and lipid complex [4]. Recently, the sheath was revealed to be assembled from a cysteine-rich peptidic glycoconjugate termed thiopeptidoglycan [5]. It has also been reported that the sheath elongates only at the ends, while the cells enclosed by the sheath grow evenly [6,7].

A thiopeptidoglycan-type sheath is also recognized in *Leptothrix cholodnii* [5], which is another well-studied sheath-forming bacterium phylogenetically related to *S. natans* [8,9]. Due to the taxonomic and ecological similarities between the genera *Sphaerotilus* and *Leptothrix*, they are collectively called the *Sphaerotilus-Leptothrix* group of bacteria [1]. Because the thiopeptidoglycan-type sheath commonly exhibits terminal elongation, a two-stage assembly mechanism was proposed for sheath formation in the *Sphaerotilus-Leptothrix* group (*S. natans* and *L. cholodnii*) [7,10]. In 2011, taxonomic descriptions of the genus *Sphaerotilus* and *S. natans* were amended, and the following species and subspecies were newly validated: *S. montanus*, *S. hippei*, *S. natans* subsp. *natans* and *S. natans* subsp. *sulfidivorans* [11]. The subspecies affiliation of *S. natans* JCM 20382 (ATCC 15291), which has been used for detailed sheath analysis, is unclear at present because it exhibits 16S rRNA gene sequence similarities ranging from 99.7 to 99.9% with both *S. natans* subsp. *natans* and *S. natans* subsp. *sulfidivorans* [11].

A new strain of *S. montanus* (ATCC-BAA-2725) with unique carbon source utilization, especially for propylene glycol (a typical de-icing compound), was found to be a consistent member of the biofilm formed in a stream contaminated with organic de-icing agents from Milwaukee

Mitchell International Airport [12]. Preliminary sugar composition analysis using gas chromatography (GC) suggested that the sheath of the strain contains glucose and galactosamine, which is the same as the sheath of *S. natans*. *S. natans* is known to have the putative glycosyl transferase gene (*sthA*) responsible for sheath formation [13]. Although a similar glycosyl transferase gene was found in *S. montanus* ATCC-BAA-2725, the similarity to *sthA* does not exceed 90% [12], suggesting that the sheath-forming polymer of *S. montanus* is slightly different from that of *S. natans*. Bacterial sheaths are microtubes assembled by the ordered aggregation of a distinctive extracellular polymer. We believe that a deeper understanding of bacterial sheaths could assist in developing biomimetic additive manufacturing (3D printing) technology. In this study, the chemical structure of the *S. montanus* sheath was determined and compared with that of the *S. natans* sheath. Furthermore, patterns of sheath elongation and cell proliferation were investigated. Because the *S. montanus* sheath was found to be free of cysteine (unlike the *S. natans* sheath), the contributions of the thiol and free amino groups to the formation and stability of the sheath are discussed.

For structural determination of the *S. monta*nus sheath, we attempted enzymatic digestion using thiopeptidoglycan lyase (DssA) [5,14,15], which is prepared from *Paenibacillus koleovorans* [16]. The enzyme can depolymerize the *S. natans* sheath into its repeating units, enabling complete structural determination of the sheath [5]. Thiopeptidoglycan lyase is suggested to be a polysaccharide lyase (EC 4.2.2) that cleaves the α-D-GalN-(1→4)-β-D-GlcA bond. It might represent a novel type of polysaccharide lyase because no polysaccharide lyase is known to cleave a linkage between non-*N*-substituted amino sugar and uronic acid residues. In validating thiopeptidoglycan lyase as a novel polysaccharide lyase, confirmation of its substrate specificity using the *S. montanus* sheath is beneficial. Characterization of thiopeptidoglycan lyase is another significant result of this study.

## 2. Materials and methods

*2.1. Bacterial strain and culture conditions*

*S. montanus* ATCC-BAA-2725 [12] was statically precultured in a medium (100 mL) composed of glucose (4 g/L), proteose peptone No. 3 (2 g/L), yeast extract (0.2 g/L), $MgSO_4 \cdot 7H_2O$ (0.2 g/L), and $CaCO_3$ (0.5 g/L) at 15 °C for 72 h. The preculture (150 μL) was inoculated into a 500-mL baffled flask containing 100 mL of a glucose-free medium composed of peptone (2 g/L), yeast extract (0.2 g/L), $MgSO_4 \cdot 7H_2O$ (0.2 g/L), and $CaCO_3$ (0.5 g/L). Cultivation was performed with agitation at 27 °C for 48 h. The filaments of *S. montanus* were harvested by centrifugation and then washed with water. The *S. natans* sheath was prepared as previously reported [17].

*2.2. Preparation and derivatization of the* S. montanus *sheath*

The washed filaments of *S. montanus* from 6 L of the culture were suspended in 20 mL of 30 mM Tris-HCl buffer (pH 8.0) containing 0.5 g/L of ethylenediaminetetraacetic acid. To the suspension, 2 mL of 10% sodium dodecyl sulfate (SDS) was added and gently mixed. After settling at 25 °C for 1 h, proteinase K (3 mg) was added to the suspension followed by vigorous shaking at 37 °C for 18 h. Then, the suspension was autoclaved at 95 °C for 1 h to complete cell lysis. By heat treatment, the sheaths formed a filmlike aggregate which was recovered and washed with water. For further purification, the sheath was soaked in 50 mM Tris-HCl buffer (pH 7.2) containing 1% SDS, incubated at 37 °C overnight, and then washed with water. To prepare a de-*O*-acetylated (weakly NaOH-treated) sheath, the sheath was suspended in 0.2 M NaOH at 4 °C for 18 h and then washed with water.

*2.3. Solubilization of the sheath*

A de-*O*-*N*-acetylated sheath-forming polymer was prepared by treating the sheath with 2 M NaOH at 37 °C for 72 h. The reaction mixture was neutralized with2 M HCl and then filtered using a glass filter (GA-55, Advantec, Tokyo, Japan). The filtrate was dialyzed against 1 mM HCl and passed through a hydrophobic cartridge (DiscoveryDSC-18 SPE, 500 mg, Merck, Darmstadt, Germany). Lyophilization was then performed to recover the de-*O*-*N*-acetylated (strongly NaOH-treated) sheath-

forming polymer. To prepare the *N*-acetylated sheath-forming polymer, de-*O*-*N*-acetylated sheath-forming polymer from 10 mg of sheath was dissolved in 10 mL of $NaHCO_3$ solution (saturated), and then 0.7 mL of acetic anhydride was gradually added while stirring [15]. After stirring for 3 h, the reaction mixture was passed through a column (2.5 × 20 cm) packed with AG50W-X8 resin ($H^+$ form, Bio-Rad, Hercules, CA, USA). The eluent was dialyzed against water and then evaporated to dryness to obtain an *N*-acetylated sheath-forming polymer.

*2.4. Reduction of uronic acid residue*

The uronic acid residue was reduced to neutral sugars based on the method described by Taylor and Conrad [18]. *N*-acetylated sheath-forming polymer (60 mg) was dissolved in 15 mL of water, and then 150 mg of 1-ethyl-3-(3-dimethylaminopropyl)-carbodiimide hydrochloride (Dojindo, Kumamoto, Japan) was gradually added at 30 °C while the solution was stirred and maintained at pH 4.5–4.8 with 0.1 M HCl using a pH controller (NPH-690D, Nissin, Tokyo, Japan). After 3.5 h of reaction time, 1-butanol (0.1 mL) was added to reduce foaming. Then, 100 mg of $NaBH_4$ was gradually added while the solution was stirred and maintained at pH 6.5–7.2 with 1 M HCl using the pH controller. After reacting for 1 h, the mixture was dialyzed (Seamless Cellulose Tubing, FUJIFILM, Tokyo, Japan) against water. The dialysate was passed through a column (1 cm × 6 cm) of AG1-X8 ($HCO_3^-$ form, Bio-Rad) to remove the uronic acid-containing sheath-forming polymer, and uronic acid-free polymer was obtained by lyophilization of the eluent.

*2.5. Size-exclusion chromatography (SEC)*

De-*O*-*N*-acetylated sheath-forming polymer (1 mg/mL in 0.1 M $Na_2SO_4$ containing 0.05 M NaCl) was subjected to SEC to determine its approximate molecular weight under the following conditions: injection volume, 20 μL; column, TSKgel G4000$PW_{XL}$ (7.8 mm × 300 mm, Tosoh, Tokyo Japan); temperature, ambient; detection, refractive index; mobile phase, 0.1 M $Na_2SO_4$; and flow rate, 0.8 mL/min. Dextrans with varied average molecular weights ($1.2 \times 10^4$, $4 \times 10^4$, $7 \times 10^4$, $1.5 \times 10^5$, 2.5

$\times 10^5$, $5.8 \times 10^5$, and $2 \times 10^6$) were used as standards.

*2.6. Chemical composition analysis*

The sample for amino acid composition analysis was hydrolyzed with 6 M HCl at 110 °C for 24 h. Amino acid composition analysis was performed using an amino acid analyzer (L-8900, Hitachi, Tokyo, Japan). The sheath and its derivatives (1 mg) for sugar composition analysis were hydrolyzed in 1 mL of 2 M trifluoroacetic acid (TFA) at 100 °C for 3 h and then evaporated. Neutral and basic monosaccharides were converted to the corresponding alditol acetates [19] and detected by GC. GC analysis was performed using a GC-2010 Plus (Shimadzu, Kyoto, Japan) equipped with a flame ionization detector under the following conditions: column, InertCap 1MS (0.25 mm × 30 m, GL Sciences); carrier gas, He; and temperature program, from 180 to 250 °C at a rate of 3 °C/min. Uronic acid was calorimetrically detected by the *m*-hydroxybiphenyl reaction [20]. The enantiomeric configurations of the sugars in the hydrolysate of the sample were determined by the formation of (*R*)-2-butylglycosides, according to the method of Gerwig et al. [21,22]. Before the reaction, 1 mg of the sample was hydrolyzed in 1 mL of 2 M TFA at 100 °C for 2 h. The butylglycosides were trimethylsilylated with TMSI-C (GL Science, Tokyo, Japan). Derivatization was also performed for D-glucose and *N*-acetyl-D-galactosamine. The derivatives were identified by GC analysis under the following conditions: column, InertCap 1MS (0.25 mm × 30 m, GL Sciences); carrier gas, He; and temperature program, from 150 to 250 °C at a rate of 3 °C/min and then maintained at 250 °C for 10 min. Note that a glycoside gives multiple peaks in GC analysis due to stereoisomers.

*2.7. Enzymatic digestion*

A thiopeptidoglycan lyase (DssA) solution was prepared as described previously [5]. To confirm the activity (eliminative reaction) of the solution, 10 μL of the solution was added to 3 mL of 25 mM Tris-HCl buffer (pH 8.0) containing 1 mg/mL of the *S. montanus* sheath (or its *N*-acetylated derivative) followed by incubation at 30 °C while the absorbance was monitored at 235 nm. After

confirmation, the sheath (30 mg) was suspended in 40 mL of the enzyme solution (25 mM Tris-HCl buffer at pH 8.0, containing the enzyme originating from 1.2 L of the liquid culture of *P. koleovorans*) followed by gentle shaking at 25 °C for 96 h. The low molecular weight fraction in the reaction mixture was recovered by ultrafiltration (Amicon Ultra-15 10K, Merck). The filtrate was concentrated to 2 mL by evaporation, and 2-propanol (20 mL) was added to insolubilize the enzymatic digest of the sheath. The digest was recovered by centrifugation, rinsed with 90% 2-propanol, and then dried under vacuum. The dried matter was treated with an ABEE labeling kit (Seikagaku Corporation, Tokyo, Japan) according to the manufacturer's instructions. The derivatives were subjected to HPLC under the following conditions: column, COSMOSIL 5$C_{18}$-AR-II (10 × 250 mm, Nacalai Tesque, Kyoto, Japan); temperature, 45 °C; mobile phase, 13.3% (v/v) acetonitrile containing 0.1% (v/v) TFA; flow rate, 2 mL/min; and detection, absorbance at 305 nm. The major ABEE derivatives were recovered by evaporation of the eluate.

*2.8. NMR spectroscopy*

Solid-state NMR $^{13}C$ cross polarization/magic angle spinning (CP/MAS) spectroscopy was performed using an Avance 600 spectrometer (Bruker, Billerica, MA, USA) at a spinning frequency of 10 000 Hz. Glycine was used as an external standard (δC 176.03) and the probe temperature was set to 25 °C. The soluble samples were dissolved in deuterium oxide together with 3-(trimethylsilyl)propionic acid (δH 0.00) and deuterated acetone (δC 31.45) as references for $^{1}H$ and $^{13}C$ chemical shifts, respectively. $^{1}H$ and $^{13}C$ NMR spectra were acquired using a DRX500 spectrometer (Bruker) at a probe temperature of 30 °C. Homo- and heteronuclear 2D spectra were acquired using the Bruker standard pulse sequences, double quantum filtered correlation spectroscopy (DQF-COSY), total correlation spectroscopy (TOCSY) (mixing times, 60 and 120 ms), nuclear Overhauser effect spectroscopy (TOCSY; mixing times, 60 and 120 ms), edited heteronuclear single quantum coherence spectroscopy (HSQC), and heteronuclear multiple bond correlation (HMBC; optimized for 5 Hz coupling constant).

*2.9. MALDI-TOF mass spectrometry*

ABEE derivatives originating from the enzymatic digest of the sheath were dissolved in water and the solution (1 μL) was mixed with 1 μL of 2,3-dihydroxybenzoic acid (DHB) solution (10 mg/mL in 30% methanol). The mixture was air-dried and subjected to matrix-assisted laser desorption/ionization-time of flight mass spectrometry (MALDI-TOF MS) analysis using Autoflex Speed (Bruker) in the following conditions: laser wavelength, 355 nm; detection mode, reflectron mode (positive); acceleration voltage, 19.00 kV (ion source 1) and 16.21 kV (ion source 2); lens, 7.6 kV; and reflectron, 21.10 kV (reflectron 1) and 9.58 kV (reflectron 2).

*2.10. Observation of the sheath's fine structure using SEM and SPM*

For scanning electron microscopy (SEM), the filament or sheath of *S. montanus* was entrapped on a membrane filter unit (SEM pore, JEOL) and washed with 20 mM phosphate buffer (pH 7.2), followed by fixation with glutaraldehyde and $OsO_4$. After stepwise dehydration with ethanol, the sample was supercritically dried in the presence of *tert*-butyl alcohol and then coated with Os, Pt, or both. Observation was conducted using a JSM-7001F microscope (JEOL). Scanning probe microscopy (SPM) was performed using an SPI 3800N (Hitachi) in tapping mode. Before observation, the sample was suspended in water and then air-dried on a silicon wafer.

*2.11. Immunostaining of the sheath*

*S. montanus* was grown at 27 °C for 18 h in an Armbruster medium [23] with agitation. The culture (3 mL) was aseptically mixed with 50 μL of 10 mM NHS-LC-LC-Biotin (Thermo Fisher Scientific, Waltham, MA, USA) and incubated for 30 min at 25 °C. The *N*-biotinylated filaments of *S. montanus* were trapped using an Ultrafree-CL filter unit (5 μm, Merck), washed with 25 mM HEPES-NaOH buffer (pH 7.2) containing 1 mg/mL of bovine serum albumin, and then suspended in 2 mL of the same buffer. The suspension (0.5 mL) was dropped onto an autoclaved glass slide (Frontier coat,

Matsunami, Osaka, Japan) and allowed to stand at 25 °C for 20 min. The glass slide with *N*-biotinylated filaments deposited on it was washed with the buffer and subsequently immunostained with a fluorescein isothiocyanate (FITC)-conjugated anti-biotin antibody (anti-Biotin-FITC, Miltenyi Biotec, Bergisch Gladbach, Germany) for 10 min. After washing with the buffer, phase-contrast and epifluorescent microscopic observations were performed using a BX51 microscope equipped with a U-MNIBA3 mirror unit (Olympus, Tokyo, Japan). For selective visualization of pre-existing regions of the sheath, *N*-biotinylated filaments fixed on the glass slide were allowed to grow in Armbruster medium at 25 °C for 3 h. After cultivation, the filaments were immunostained for microscopy.

### *2.12. Phase contrast microscopy of* S. montanus *microculture*

A grid pattern (1.5 $cm^2$), approximately 3 mm high, was formed with petroleum jelly on a glass slide (Frontier coat, Matsunami) and then irradiated with ultraviolet light for 15 min. *S. montanus* preculture (0.3 mL, grown in glucose-free medium) was aseptically poured into the grid on the slide. Excess culture fluid was removed, and the filaments fixed on the slide were washed with glucose-free medium. The medium was added to the grid, and the grid was then covered with a sterilized 1.8 $cm^2$ coverslip that allowed an air bubble to occupy approximately one-third of the grid. The microculture was intermittently observed by phase-contrast microscopy using an inverted microscope (DMI3000B, Leica, Wetzlar, Germany) at 25 °C.

## 3. Results

### *3.1. Preparation of the sheath*

In a previous study [12], preparation of the *S. montanus* sheath was attempted, using the procedures optimized for *S. natans*. In this study, we found that better growth of *S. montanus* was achieved by replacing protease-peptone No. 3 with peptone. We also found that deformation of the *S. montanus* sheath occurs during repetitive heat treatment at 110 °C (which is included in the sheath isolation

protocol for *S. natans*) [17]. Considering the heat susceptibility of the *S. montanus* sheath, a modified protocol with heat treatment at 95 °C was developed as described in section 2.2. Before the treatments using the modified protocol, the cells enclosed with the sheath were clearly observed by phase contrast (Fig. 1a), SEM (Fig. 1c), and SPM (Fig. 1e) microscopies. After the treatments, the cells were completely removed and the sheath of the original microtube structure was obtained as shown in the phase contrast (Fig. 1b), SEM (Fig. 1d), and SPM (Fig. 1f) micrographs. The yield of the sheath from the *S. montanus* filaments by dry weight was approximately 10%. In the SEM micrograph of *S. montanus*, fibrous material was observed outside the sheath (Fig. 1c). This material was likely observed as slime surrounding the sheath in the SPM image (Fig. 1e). Because the purified sheath has no surrounding material (Fig. 1b, f), the fiber or slime is likely removable by sheath isolation treatments. Although the cultures (both liquid and solid) of *S. montanus* were not sticky, the strain was found to secrete a small amount of mucous polymer in addition to the sheath-forming polymer.

### *3.2. Solid-state NMR spectroscopy of the sheath*

Fig. 2a shows the $^{13}$C-CP/MAS spectrum of the *S. montanus* sheath. The major component of the sheath was expected to be sugar because the signals typical of anomeric carbon (approximately 100 ppm) and carbons bearing a hydroxy group (40–90 ppm) were strongly detected. In addition to these signals, two major methyl carbon signals, likely part of an acetyl group, were detected at 20–35 ppm. The presence of the acetyl group was supported by a carbonyl carbon signal at 174 ppm. Because the sheath was positive in the *m*-hydroxybiphenyl reaction, this signal was also assigned to the carboxyl group in the uronic acid residue. Overall, the $^{13}$C-CP/MAS spectrum of the *S. montanus* sheath was similar to that of the *S. natans* sheath (Fig. 2b), suggesting that both sheath-forming polymers have the same polysaccharide backbone. When the *S. montanus* sheath was de-*O*-acetylated with 0.2 M NaOH, the methyl carbon signal at 30 ppm was diminished while other signals, including another methyl carbon signal at 23 ppm, were not affected (Fig. 2c). This suggests that the signals at 30 ppm and 23 ppm arose from the *O*-acetyl and *N*-acetyl groups, respectively. Both the methyl carbon signals

and the carbonyl carbon signal were diminished by de-*O*-*N*-acetylation with 2 M NaOH (Fig. 2d). When the completely deacetylated derivative was *N*-acetylated, the carbonyl carbon signal and the methyl carbon signal at 23 ppm intensified without regeneration of the signal at 30 ppm (Fig. 2e). Based on these results, the *S. montanus* sheath was expected to be mainly composed of *O*- and *N*-acetylated polysaccharides containing uronic acid, similar to the *S. natans* sheath. It should also be noted that the de-*O*-acetylated polymer was insoluble in water, the de-*O*-*N*-acetylated polymer was water soluble regardless of pH, and the *N*-acetylated polymer was water soluble only under basic conditions. The molecular weight of the de-*O*-*N*-acetylated polymer was estimated to be $5.2 \times 10^5$ by SEC (Fig. S1). The molecular weight of the solubilized (hydrazinolyzed) sheath of *S. natans* is reported to be $1.2 \times 10^5$ [16]. We assumed that the molecular weights of the sheath-forming polymers of *Sphaerotilus* strains are commonly in the range of $10^5$.

### *3.3. Chemical composition of the sheath*

To identify uronic acid, the sheath was reduced to convert the uronic acid residues to the corresponding neutral sugar residues. In GC analysis of alditol acetates derived from the hydrolysates of the non-treated sheath (Fig. S2a) and the reduced derivatives (Fig. S2b), glucose (19 min) and galactosamine (24 min) were commonly detected. Because the relative abundance of glucose was higher in the derivative (Fig. S2a, b), the uronic acid was identified as glucuronic acid. Absolute configuration analysis of the reduced derivative demonstrated that the sheath contained D-glucose, D-galactosamine, and D-glucuronic acid (Fig. S3). The relative amino acid compositions of the *S. montanus* and *S. natans* sheaths are summarized in Table S1. In contrast to *S. natans*, which is rich in glycine and cysteine, only traces of cysteine were detected in the *S. montanus* sheath. Although the glycine and glutamic acid (or glutamine) contents were relatively high, their absolute amounts could not be determined using this method, and the possibility remains that they originated from impurities.

### *3.4. NMR analysis of the* N*-acetylated derivative*

The *S. montanus* sheath was found to be solubilized by deacetylation and subsequent *N*-acetylation allowing for solution-state NMR analysis. In the 1D-$^{1}$H NMR spectrum of the *N*-acetylated derivative (Fig. 3), five anomeric proton (H1) signals were detected, suggesting that the derivative has a pentasaccharide repeating unit. The sugar residues in the unit were temporarily designated **A–E** as indicated in Fig. 3. In addition, a weak unidentified signal (temporarily designated **X**-H1) was detected at 4.98 ppm beside the **B**-H1 signal (4.93 ppm). A similar weak signal can be found in the former 1D-$^{1}$H NMR spectra of the solubilized derivatives of the *S. natans* sheath [5,24]. The H2 signal of each sugar residue in the *N*-acetylated derivative was assigned by the DQF-COSY experiment (Fig. S4). The $^{3}J_{1,2}$ values of residues **A** and **B** were too small to be determined, suggesting that these residues are the α anomer. Because the $^{3}J_{1,2}$ values of residues **C**, **D**, and **E** were greater than 6 Hz, these residues were believed to be the β anomer. Three acetyl proton signals were detected and their intensity relative to **A**-H1 was approximately 9 in total, indicating that the unit has three acetyl groups. In the 1D-$^{13}$C NMR spectrum of the *N*-acetylated derivative (Fig. S5), five anomeric carbon (C1) signals were detected, confirming that the derivative consisted of a pentasaccharide repeating unit. Four major signals were detected in the carbonyl carbon region (Fig. S5), which is in agreement with the one carboxyl group (glucuronic acid residue) and three acetyl groups found in the repeating unit. Three signals were observed in the nitrogen-bearing carbon region (Fig. S5), revealing the incorporation of three amino groups (three amino sugar residues) in the repeating unit. Further assignment was performed using NOESY, TOCSY (Fig. S6), edited HSQC (Fig. S7), and HMBC (Fig. S8) experiments. In the HSQC spectrum (Fig. S7), **X**-H1 exhibited correlation with **B**-C1, suggesting that **X**-H1 is another (minor) signal of **B**-H1. Supporting this assumption, HMBC correlations with **B**-C2, **B**-C3, **B**-C5, and **A**-C4 were detected on the track of **X**-H1 (Fig. S8). Likewise, correlations of **X**-H1 with the proton signals of residue **B** were observed in DQF-COSY (Fig. S4) and TOCSY experiments (Fig. S6). Residues **A**, **B**, and **D** were revealed to be galactosamine residues because **A**-C2, **B**-C2, and **D**-C2 were detected within the nitrogen-bearing carbon region (around 50 ppm). Residue **C** was indicated as a glucuronic acid residue because one of the four

carbonyl carbon signals exhibited HMBC correlations with **C**-H4 and **C**-H5 (Fig. S8). The other three carbonyl carbons correlated to **A**-H2, **B**-H2, and **D**-H2, confirming that residues **A**, **B**, and **D** are GalNAc. The positions of glycosidic linkages and the formation of pyranose rings in all residues were confirmed by NOESY and HMBC (Fig. S8) spectra. Based on these results, the *N*-acetylated derivative was determined to be [4)-β-D-GlcA*p*-(1→4)-β-D-Glc*p*-(1→3)-β-D-GalN*p*Ac-(1→4)-α-D-GalN*p*Ac-(1→4)-α-D-GalN*p*-(1→]$_n$. The assignment of the $^1$H and $^{13}$C NMR signals is summarized in Table 1.

*3.5. Enzymatic degradation of the sheath*

The *S. montanus* sheath was successfully degraded by thiopeptidoglycan lyase (DssA). In contrast, relative activity on the *N*-acetylated sheath was only about 8% (Fig. S9), revealing that the enzyme specifically cleaves a non-*N*-substituted bond, α-D-GalN-(1→4)-β-D-GlcA. Enzymatic digests recovered from the reaction mixture were derivatized with ABEE, and the derivatives were then subjected to HPLC (Fig. S10). Two major derivatives in nearly equal amounts (peak areas) were detected at 20 min (derivative I) and 29 min (derivative II), then recovered and subjected to structural analysis. In their 1D-$^1$H NMR spectra (Fig. 4a), aryl proton (6.8 and 7.9 ppm) and methyl proton (1.4 ppm) signals typical for ABEE [25] were observed in addition to the signals typical for sugar residues (3.5–5.5 ppm). An olefinic proton signal (5.7–5.8 ppm) was observed in both spectra. This signal can be assigned to H4 of the unsaturated β-glucuronic acid residue (4-deoxy-β-L-*threo*-hex-4-enopyranuronic acid, β-ΔGlcA) generated by the action of DssA. Accordingly, both derivatives are expected to have a sequence of ΔGlcA-Glc-GalNAc-GalNAc-GalNr-ABEE (note that GalNr is an abbreviation for reduced GalN residue). In the acetyl proton region (around 2 ppm), three and four signals were observed in derivatives I and II, respectively (Fig. 4b). Accordingly, derivatives I and II was revealed to have three and four acetyl groups, respectively. The assigned ions for the MALDI-TOF MS spectrum of each derivative are shown in Fig. 5. Adduct molecular ions $[M+Na]^+$ (*m/z* 1119.4) and $[M+K]^+$ (*m/z* 1135.4) were detected from derivative I (Fig. 5a). Adduct ions [M-

ΔGlcA+Na]$^+$ (*m/z* 961.4) and [M-ΔGlcA +K]$^+$(*m/z* 977.3) were also detected. The removal of ΔGlcA might be due to the degradation of this residue. These ions suggest that derivative I has one *O*-acetyl group within Glc-GalNAc-GalNAc-GalNr. From derivative II, adduct molecular ions [M+Na]$^+$ (*m/z* 1161.4) and [M+K]$^+$ (*m/z* 1177.4) were detected (Fig. 5b). Adduct ions [M-ΔGlcA+Na]$^+$ (*m/z* 1003.4) and [M-ΔGlcA+K]$^+$ (*m/z* 1019.4) were also detected, suggesting that derivative II has two *O*-acetyl groups within Glc-GalNAc-GalNAc-GalNr. Thus, the difference in the acetylation degree between the derivatives was confirmed by MALDI-TOF MS analysis. It is possible that derivative II has an additional *O*-acetyl group because it exhibits a longer retention time (higher hydrophobicity) in the reverse-phase HPLC (Fig. S10). To determine the positions of *O*-acetylation in derivative I, DQF-COSY (Fig. S11), TOCSY (Fig. S12), NOESY, edited HSQC (Fig. 6a), and HMBC (Fig. 6b) experiments were attempted. Most of the signals were assigned as indicated in the figures. In these experiments, the abbreviations **A**r (GalNr), **B** (α-GalNAc), d**C** (β-ΔGlcA), **D** (β-GalNAc), and **E** (β-Glc) were used. The unidentified peaks might be due to an impurity because the HPLC peak of derivative I was slightly shouldered (Fig. S10). The HSQC signals observed in the acetyl proton region (around 2 ppm) exhibited HMBC correlations with carbonyl carbons (Fig. 6b). On the tracks of these carbonyl carbons, correlations with **E**-H3 (position 3 of β-Glc), **D**-C2 (position 2 of β-GalNAc), and **B**-C2 (position 2 of α-GalNAc) were observed (Fig. 6b). Thus, derivative I was revealed to be *O*-acetylated at position 3 of β-D-Glc. Similarly, derivative II was subjected to DQF-COSY (Fig. S13), TOCSY (Fig. S14), NOESY, edited HSQC (Fig. 15a), and HMBC (Fig. 15b) experiments. In the acetyl proton region of the edited HSQC spectrum (Fig. S15a), four signals were detected. As expected, these signals correlated to the carbonyl carbons in the HMBC experiment (Fig. S15b). On the tracks of these carbonyl carbons, correlations to **B**-H3 (position 3 of α-GalNAc), **E**-H3 (position 3 of β-Glc), **D**-C2 (position 2 of β-GalNAc), and **B**-C2 (position 2 of α-GalNAc) were observed (Fig. S15b). Thus, derivative II was revealed to be *O*-acetylated at position 3 of β-D-Glc and position 3 of α-GalNAc. Consequently, the structures of derivatives I and II were determined as shown in Fig. 7a and b. The assigned $^1$H and $^{13}$C NMR signals are summarized in Table 2. Because the peak

areas of the derivatives in HPLC were almost the same (Fig. S10), the β-D-Glc and α-D-GalNAc in the sheath-forming polymer are assumed to be stoichiometrically and substoichiometrically 3-*O*-acetylated, respectively. Based on this assumption, the sheath-forming polymer of *S. montanus* was concluded to be a partially 3-*O*-acetylated polysaccharide with the following repeating unit: [→4)-β-D-GlcA-(1→4)-β-D-Glc-(1→3)-β-D-GalNAc-(1→4)-α-D-GalNAc-(1→4)-α-D-GalN-(1→] (Fig. 7c). The assigned $^{1}$H and $^{13}$C NMR signals are summarized in Table 2.

*3.6. Elongation pattern of the sheath*

Because the *S. montanus* sheath was confirmed to have free amino groups, the sheath of viable *S. montanus* filaments was subjected to *N*-biotinylation. The filaments were immunostained with a fluorescent anti-biotin antibody. The filaments exhibited florescence, allowing easy distinction of the sheath from the inside cells by epifluorescence microscopy (Fig. 8a). The epifluorescent image of the tip of the filaments clearly shows that the sheath has an open end (Fig. 8a). In addition, diminishing fluorescence at the ends suggests that the sheath in the terminal regions is thin and under construction. Even after *N*-biotinylation, the filaments maintained their viability, and fluorescence in the full filaments was localized to the middle regions (Fig. 8b), confirming that the sheath elongates at its terminal regions. As indicated in the serial phase-contrast images of a viable *S. montanus* filament (Fig. S16), the cells elongated and divided at a similar rate regardless of their position in the sheath.

## 4. Discussion

In this study, the *S. montanus* sheath was found to have a fine nonwoven fabric-like structure. It was also revealed that the sheath has open ends and elongates at its terminal regions, while the cells proliferate evenly regardless of their position in the sheath. These morphological and physiological properties are commonly recognized in *S. natans* [6,7,26] and *L. cholodnii* [10,27,28]. For these bacteria, a two-stage sheath-forming mechanism, which comprises a nanofibril formation stage and a nanofibril aggregation stage, has been proposed [7,10]. More recently, the loose entanglement of

extracellular nanofibrils and subsequent tight aggregation (sheath formation) in the terminal section of the *L. cholodnii* filament were clearly visualized by atmospheric SEM [28], supporting this hypothesis. Presumably, *S. montanus* has the same sheath-forming mechanism. *S. natans* and *L. cholodnii* sheaths are commonly assembled from thiopeptidoglycan, which consists of polysaccharide chains covalently linked to peptide chains rich in thiol groups [5,29].

The structure of the sheath-forming polymer of *S. montanus* was found to be essentially the same as that of *S. natans* (Fig. 7c, d). However, the *S. montanus* polymer is free of amino acids and is not in the category thiopeptidoglycans but instead is an amphoteric glycan. Although the *S. montanus* polymer cannot form intermolecular disulfide bonds (unlike the *S. natans* and *L. cholodnii* polymers), it can still form sheaths, revealing that disulfide linkage is not essential for sheath formation. Considering that the *S. montanus* sheath is less heat stable than the *S. natans* sheath, the disulfide bonds in the thiopeptidoglycan-type sheaths likely provide stabilization or reinforcement. Consequently, the contribution of disulfide linkage in sheath formation was found to be smaller than previously expected [5,17,27,29,30]. It was also found that the *Sphaerotilus-Leptothrix* sheaths can be categorized as either peptide-containing (thiopeptidoglycan-based) or peptide-free (glycan-based). Because *S. natans* and *L. cholodnii* filaments can be stained with thiol-specific fluorescent reagents [7,10,27], these reagents allow convenient distinction between their filaments and those of *S. montanus*.

As shown in Fig. 7, the sheath-forming polymers of both *S. natans* and *S. montanus* have one carboxy group (GlcA) and one amino group (GalN) in their repeating units, allowing inner molecular charge neutralization and intermolecular electrostatic interaction, which might be required for sheath formation. The *S. natans* polymer is substoichiometrically *O*-acetylated and bound with *N*-acetyl-L-cysteinylglycine side chains; in contrast, in the *S. montanus* polymer, the corresponding positions are stoichiometrically *O*-acetylated and *N*-acetylated, respectively. The *S. montanus* polymer has an additional substoichiometric acetylation at position 3 of α-GalNAc as if to compensate for the dipeptide side chain. Because deacetylation (removal of *O*- and *N*-acetyl groups) causes

solubilization of the *S. montanus* polymer, the acetyl groups are apparently involved in intermolecular interaction to form the sheath, as shown in Fig. S17. Even after *N*-acetylation (elimination of free amino groups), the deacetylated polymer is soluble, especially under basic conditions. However, *N*-acetylation without prior deacetylation did not cause solubilization of the *S. montanus* polymer, even under basic conditions. This demonstrates that the contribution of *O*-acetyl groups in sheath formation probably increases the capacity for hydrogen bonding and hydrophobic interactions. Biological (enzymatic) modifications (de-*N*-acetylation and *O*-acetylation) of extracellular polysaccharides are known to occur after secretion [31,32]. Therefore, together with intercellular glycosyl transferases such as SthA (which is responsible for sheath formation), periplasmic de-*N*-acetylase and *O*-acetylase are assumed to be indispensable for sheath formation (i.e., for the production of mature sheath-forming polymer) [13].

Another achievement of this work is the additional confirmation of the substrate specificity of DssA (thiopeptidoglycan lyase). It was found that DssA acts not only on the *S. natans* sheath but also on the *S. montanus* sheath, demonstrating that DssA activity is not affected by the *N*-acetyl-L-cysteinylglycine side chain (Fig. 7c, d). It was also found that DssA is more specific for α-D-GalN-(1→4)-β-D-GlcA linkage than for α-D-GalNAc-(1→4)-β-D-GlcA linkage (Fig. S9). Consequently, DssA can be defined as a polysaccharide lyase that catalyzes eliminative cleavage of α-D-galactosaminopyranosyl-(1→4)-β-D-glucopyranosyluronate bonds of the thiopeptidglycan backbone or related polysaccharides, releasing pentasaccharides containing a 4-deoxy-4,5-unsaturated D-glucopyranosyluronic acid at the non-reducing end. Polysaccharide lyase (EC 4.2.2) comprises 26 types of lyases (EC 4.2.2.1 – EC 4.2.2.3, EC 4.2.2.5 – EC 4.2.2.27). Among them, EC 4.2.2.1, EC 4.2.2.5, and EC 4.2.2.19 – EC 4.2.2.21 cleave linkages between *N*-substituted amino sugar and uronic acid residues. The specificity of thiopeptidoglycan lyase is clearly distinguishable from these known polysaccharide lyases based on its specificity to the linkage between non-*N*-substituted amino sugar and uronic acid residues. Moreover, no gene exhibiting meaningful similarity to the thiopeptidoglycan lyase gene (*dssA*, AB084782) at full length was found in our database searches [14];

thiopeptidoglycan lyase does not exhibit significant similarity to known lyase genes at full length. We believe that thiopeptidoglycan lyase (DssA) represents a new category of polysaccharide lyase.

## 6. Acknowledgments

The authors acknowledge the use of NMR spectrometers due to the support of the Joint Usage/Research Program on Zero-Emission Energy Research at the Institute of Advanced Energy, Kyoto University (ZE2021A-09). This work was supported by a Grant-in-Aid for Scientific Research (C) 20K05846 from the Japan Society for the Promotion of Science. The funding source played no role in the study design; in the collection, analysis, and interpretation of data; in the writing of the report; or in the decision to submit the article for publication.

## 7. Declaration of interest

We confirm that the manuscript has been read and approved by all named authors and that there are no other persons who satisfied the criteria for authorship but are not listed. We further confirm that the order of authors listed in the manuscript has been approved by all of authors.

## References

[1] W.L. van Veen, E.G. Mulder, M.H. Deinema, The *Sphaerotilus-Leptothrix* group of bacteria, Microbiol. Rev. 42 (1978) 329−356.

[2] D. Jenkins, M.G. Richard, G.T. Daigger, Manual on the causes and control of activated sludge bulking and forming, second ed., Lewis Publishers, Chelsea, Michigan, 1993.

[3] A.M. Martins, K. Pagilla, J.J. Heijnen, M.C. van Loosdrecht, Filamentous bulking sludge—a critical review, Water Res. 38 (2004) 793−817.

[4] A.H. Romano, J.P. Peloquin, Composition of the sheath of *Sphaerotilus natans*, J. Bacteriol. 86 (1963) 252−258.

[5] K. Kondo, M. Takeda, W. Ejima, Y. Kawasaki, T. Umezu, M. Yamada, J. Koizumi, T. Mashima,

M. Katahira, Study of a novel glycoconjugate, thiopeptidoglycan, and a novel polysaccharide lyase, thiopeptidoglycan lyase, Int. J. Biol. Macromol. 48 (2011) 256−262.

[6] A.H. Romano, D.J. Geason, Pattern of sheath synthesis in *Sphaerotilus natans*, J. Bacteriol. 88 (1964) 1145−1150.

[7] M. Takeda, T. Umezu, Y. Kawasaki, S. Shimura, K. Kondo, J. Koizumi, A spatial relationship between sheath elongation and cell proliferation in *Sphaerotilus natans*, Biosci. Biotechnol. Biochem. 76 (2012) 2357−2359.

[8] P.L. Siering, W.C. Ghiorse, Phylogeny of the *Sphaerotilus-Leptothrix* group inferred from morphological comparisons, genomic fingerprinting, and 16S ribosomal DNA sequence analyses, Int. J. Syst. Bacteriol. 46 (1996) 173−182.

[9] P.L. Siering, W.C. Ghiorse, Development and application of 16S rRNA-targeted probes for detection of iron- and manganese-oxidizing sheathed bacteria in environmental samples, Appl. Environ. Microbiol. 63 (1997) 644−651.

[10] M. Takeda, Y. Kawasaki, T. Umezu, S. Shimura, M. Hasegawa, J. Koizumi, Patterns of sheath elongation, cell proliferation, and manganese(II) oxidation in *Leptothrix cholodnii*, Arch. Microbiol. 194 (2012) 667−673.

[11] E. Gridneva, E. Chernousova, G. Dubinina, V. Akimov, J. Kuever, E. Detkova, M. Grabovich, Taxonomic investigation of representatives of the genus *Sphaerotilus*: descriptions of *Sphaerotilus montanus* sp. nov., *Sphaerotilus hippei* sp. nov., *Sphaerotilus natans* subsp. *natans* subsp. nov. and *Sphaerotilus natans* subsp. *sulfidivorans* subsp. nov., and an emended description of the genus *Sphaerotilus*, Int. J. Syst. Evol. Microbiol. 61 (2011) 916−925.

[12] M.A. Nott, H.E. Driscoll, M. Takeda, M. Vangala, S.R. Corsi, S. W. Tighe, Advanced biofilm analysis in streams receiving organic deicer runoff. PLoS One. 15 (2020) e0227567.

[13] T. Suzuki, T. Kanagawa, Y. Kamagata, Identification of a gene essential for sheathed structure formation in *Sphaerotilus natans*, a filamentous sheathed bacterium, Appl. Environ. Microbiol. 68 (2002) 365–371.

[14] M. Takeda, K. Nishina, Y. Hanaoka, M. Higo, M. Terui, I. Suzuki, J. Koizumi, A novel gene encoding an enzyme that degrades a polysaccharide from the sheath of *Sphaerotilus natans*, Biosci. Biotechnol. Biochem. 67 (2003) 2300−2303.

[15] M. Takeda, K. Iohara, S. Shinmaru, I. Suzuki, J. Koizumi, Purification and properties of an enzyme capable of degrading the sheath of *Sphaerotilus natans*, Appl. Environ. Microbiol. 66 (2000) 4998−5004.

[16] M. Takeda, Y. Kamagata, S. Shinmaru, T. Nishiyama, J. Koizumi, *Paenibacillus koleovorans* sp. nov., able to grow on the sheath of *Sphaerotilus natans*, Int. J. Syst. Evol. Microbiol. 52 (2002) 1597−1601.

[17] M. Takeda, F. Nakano, T. Nagase, K. Iohara, J. Koizumi, Isolation and chemical composition of the sheath of *Sphaerotilus natans*, Biosci. Biotechnol. Biochem. 62 (1998) 1138−1143.

[18] R.L. Taylor, H. E. Conrad, Stoichiometric depolymerization of polyuronides and glycosaminoglycuronans to monosaccharides following reduction of their carbodiimide-activated carboxyl groups, Biochemistry 11 (1972) 1383−1388.

[19] R.K. Merkle, I. Poppe, Carbohydrate composition analysis of glycoconjugates by gas-liquid chromatography/mass spectrometry, in: W.J. Lennarz, G.W. Hart (Eds.), Methods in Enzymology Vol. 230, Academic Press, San Diego, 1994, pp. 1–15.

[20] T.M. Filisetti-Cozzi, N.C. Carpita, Measurement of uronic acids without interference from neutral sugars, Anal. Biochem. 197 (1991) 157−162.

[21] G.J. Gerwig, J.P. Kamerling, J.F.G. Vliegenthart, Determination of the D and L configuration of neutral monosaccharides by high-resolution capillary G.L.C., Carbohydr. Res. 62 (1978) 349−357.

[22] G.J. Gerwig, J.P. Kamerling, J.F.G. Vliegenthart, Determination of the absolute configuration of monosaccharides in complex carbohydrates by capillary G.L.C., Carbohydr. Res. 77 (1979) 1−7.

[23] E.H. Armbruster, Improved technique for isolation and identification of *Sphaerotilus*, Appl. Microbiol. 17 (1969) 320–321.

[24] M. Takeda, T. Nakamori, M. Hatta, H. Yamada, J. Koizumi J, Structure of the polysaccharide isolated from the sheath of *Sphaerotilus natans*, Int. J. Biol. Macromol. 33 (2003) 245−250.

[25] M. Takeda, K. Kondo, R. Tominaga, H. Mori, M. Kato, R. Usami, T. Murakami, K. Ueda, I. Suzuki, M. Katahira, Aggregability of β(1→4)-linked glucosaminoglucan originating from a sulfur-oxidizing bacterium *Sphaerotilus natans*, Biosci. Biotechnol. Biochem. 84 (2020) 2085−2095.

[26] J.F. Hoeniger, H.D. Tauschel, J.L. Stokes, The fine structure of *Sphaerotilus natans*, Can. J. Microbiol. 19 (1973) 309−313.

[27] D. Emerson, W.C. Ghiorse, Ultrastructure and chemical composition of the sheath *of Leptothrix discophora* SP-6, J. Bacteriol. 175 (1993) 7808−7818.

[28] T. Kunoh, K. Morinaga, S. Sugimoto, S. Miyazaki, M. Toyofuku, K. Iwasaki, N. Nomura, A.S Utada, Polyfunctional nanofibril appendages mediate attachment, filamentation, and filament adaptability in *Leptothrix cholodnii*, ACS Nano 14 (2020) 5288−5297.

[29] M. Takeda, K. Kondo, M. Yamada, J. Koizumi, T. Mashima, A. Matsugami, M. Katahira, Solubilization and structural determination of a glycoconjugate which is assembled into the sheath of *Leptothrix cholodnii*, Int. J. Biol. Macromol. 46 (2010) 206−211.

[30] D. Emerson, W.C. Ghiorse, Role of disulfide bonds in maintaining the structural integrity of the sheath of *Leptothrix discophora* SP-6. J. Bacteriol. 175 (1993) 7819−7827.

[31] D.J. Little, G. Li., C. Ing, B.R. DiFrancesco, N.C. Bamford, H Robinson, M. Nitz, R. Pomès, P.L. Howell, Modification and periplasmic translocation of the biofilm exopolysaccharide poly-β-1,6-*N*-acetyl-D-glucosamine, PNAS 111 (2014) 11013–11018.

[32] M. Pauly, V. Ramírez, New insights into wall polysaccharide *O*-acetylation, Front. Plant Sci. 9 (2018) 1210.

**Table 1**. $^{1}H$ and $^{13}C$ resonance assignments (δ in ppm)

| Residue | Nucleus | 1 ($^{3}J_{1,2}$, Hz) | 2 | 3 | 4 | 5 | 6 (6′) | NAc |
|---|---|---|---|---|---|---|---|---|
| α-GalNAc (**A**) | $^{1}H$ | 5.10 | 4.29 | 4.00 | 4.05 | 3.95 | 3.65 (3.69) | 2.05 |
| | $^{13}C$ | 96.0 | 52.4 | 69.9 | 79.3 | 74.6 | 62.8 | 24.0, 177.4 |
| α-GalNAc (**B**) | $^{1}H$ | 4.93[a] | 4.17 | 4.16 | 4.23 | 4.37 | 3.62 (3.86) | 2.07 |
| | $^{13}C$ | 101.2 | 53.0 | 70.1 | 78.2 | 73.0 | 63.3 | 24.0, 177.0 |
| β-GlcA (**C**) | $^{1}H$ | 4.78 (8.4) | 3.53 | 4.39 | 3.85 | 4.20 | - | - |
| | $^{13}C$ | 102.9 | 72.8 | 69.6 | 75.0 | 76.7 | 178.3 | - |
| β-GalNAc (**D**) | $^{1}H$ | 4.76 (6.6) | 4.03 | 3.93 | 4.16 | 3.69 | 3.77 (3.81) | 2.01 |
| | $^{13}C$ | 104.9 | 54.3 | 82.7 | 70.9 | 77.4 | 63.8 | 24.0, 177.6 |
| β-Glc (**E**) | $^{1}H$ | 4.52 (7.2) | 3.35 | 3.63 | 3.62 | 3.55 | 3.81 (3.91) | - |
| | $^{13}C$ | 106.8 | 75.4 | 76.8 | 81.3 | 77.4 | 62.8 | - |

[a]A minor signal was detected at 4.98 ppm.

**Table 2**. $^{1}H$ and $^{13}C$ resonance assignments of ABEE derivatives (δ in ppm)

| *Derivative I* | | | | | | | | | |
|---|---|---|---|---|---|---|---|---|---|
| Sugar residue | Nucleus | 1 | 2 | 3 | 4 | 5 | 6 (6′) | NAc | OAc |
| β-ΔGlcA (d**C**) | $^{1}H$ | 5.16 | 3.86 | 4.34 | 5.71 | - | - | - | - |
| | $^{13}C$ | 101.5 | 67.9 | 65.1 | 110.3 | 147.2 | ND[a] | - | - |
| β-Glc (**E**) | $^{1}H$ | 4.58 | 3.55 | 4.94 | 4.06 | 3.60 | 3.93 (3.79) | - | 2.09 |
| | $^{13}C$ | 106.8 | 74.0 | 77.8 | 75.3 | 77.7 | 62.7 | - | 23.2, 176.7 |
| β-GalNAc (**D**) | $^{1}H$ | 4.70 | 3.99 | 3.89 | 4.18 | 3.65 | 3.80 (3.80) | 1.98 | - |
| | $^{13}C$ | 104.6 | 54.1 | 83.0 | 70.6 | 77.3 | 63.5 | 25.1, 177.6 | - |
| α-GalNAc (**B**) | $^{1}H$ | 5.04 | 4.13 | 3.84 | 4.00 | 3.87 | 3.69 (3.66) | 2.04 | - |
| | $^{13}C$ | 101.4 | 52.7 | 70.3 | 78.0 | 74.0 | 64.0 | 24.7, 177.1 | - |
| α-GalNAc (**Ar**) | $^{1}H$ | 3.59 | 3.70 | 4.09 | 3.91 | 3.96 | 3.65 (3.65) | - | - |
| | $^{13}C$ | 45.3 | 53.5 | 71.6 | 80.8 | 73.8 | 64.8 | - | - |
| Nonsugar residue | Nucleus | $CH_2$ | $CH_3$ | C=O | 1 | 2, 6 | 3, 5 | 4 | |
| ABEE | $^{1}H$ | 4.35 | 1.37 | - | 7.89 | 6.81 | 7.91 | - | |
| | $^{13}C$ | 64.5 | 16.3 | 171.9 | 121.1 | 115.0 | 134.3 | 154.7 | |
| *Derivative II* | | | | | | | | | |
| Sugar residue | Nucleus | 1 | 2 | 3 | 4 | 5 | 6 (6′) | NAc | OAc |
| β-ΔGlcA (d**C**) | $^{1}H$ | 5.17 | 3.88 | 4.35 | 5.82 | - | - | - | - |
| | $^{13}C$ | 101.8 | 67.8 | 65.0 | 112.3 | 145.6 | 170.0 | - | - |
| β-Glc (**E**) | $^{1}H$ | 4.60 | 3.53 | 4.94 | 4.04 | 3.59 | 3.92 (3.79) | - | 2.08 |
| | $^{13}C$ | 106.6 | 74.0 | 77.9 | 75.6 | 77.5 | 62.7 | - | 23.2, 176.7 |
| β-GalNAc (**D**) | $^{1}H$ | 4.48 | 3.89 | 4.01 | 4.18 | 3.59 | 3.77 (3.67) | 2.01 | - |
| | $^{13}C$ | 104.5 | 54.3 | 82.2 | 70.2 | 77.0 | 63.5 | 25.0, 177.6 | - |
| α-GalNAc (**B**) | $^{1}H$ | 5.06 | 4.36 | 4.90 | 3.96 | 3.81 | 3.68 (3.60) | 1.97 | 2.14 |
| | $^{13}C$ | 101.1 | 50.7 | 72.6 | 76.1 | 73.9 | 63.6 | 24.5, 176.8 | 22.9, 175.9 |
| α-GalNAc (**Ar**) | $^{1}H$ | 3.61 | 3.73 | 4.11 | 3.94 | 3.97 | 3.64 (3.64) | - | - |
| | $^{13}C$ | 44.9 | 53.3 | 70.6 | 80.5 | 73.6 | 64.8 | - | - |
| Nonsugar residue | Nucleus | $CH_2$ | $CH_3$ | C=O | 1 | 2, 6 | 3, 5 | 4 | |
| ABEE | $^{1}H$ | 4.32 | 1.35 | - | 7.89 | 6.82 | 7.92 | 4.32 | |
| | $^{13}C$ | 64.4 | 16.4 | 172.0 | 121.4 | 115.2 | 134.5 | 154.4 | |

[a]ND: Not detected.

Figure legends

Fig. 1. Micrographs of the filament (a, c, e) and purified sheath (b, d, f) of *S. montanus*. *S. montanus* filaments grown on glucose-free medium were observed using phase-contrast microscopy (a). The suspension of the sheath was observed using phase-contrast microscopy (b). The membrane filter attached to the filament (c) or sheath (b) was fixed and metal coated for observation using scanning electron microscopy. The filament (e) or sheath (f) airdried on a silicon wafer was subjected to scanning probe microscopy.

Fig. 2. $^{13}C$ cross polarization/magic angle spinning spectra of the *Sphaerotilus* sheaths (a, b) and the derivatives of the *S. montanus* sheath (c, d, e). The lyophilized samples were subjected to analysis at 25 °C. The spectra of the purified sheaths of *S. montanus* (a) and *S. natans* (b) are compared in the left column. In the right column, the spectra of de-*O*-acetylated (c), de-*O*-*N*-acetylated (d), and *N*-acetylated (e) derivatives of the *S. montanus* sheath are shown. Important signals are indicated by C=O (carbonyl carbon signal), Anomeric (anomeric carbon signal) and Ac (methyl carbon signal due to acetyl group).

Fig. 3. 1D-$^{1}H$ NMR spectrum of the *N*-acetylated derivative of the *S. montanus* sheath. The solution (approximately 5 mg/mL) of the *N*-acetylated derivative was subjected to analysis at 30 °C. Important signals are indicated by arrows. Note that a weak unidentified signal (**X**-H1) was detected in the anomeric proton region. Relative intensities are indicated in the parentheses.

Fig. 4. 1D-$^{1}H$ NMR spectra of the ABEE derivatives. The solutions (approximately 5 mg/mL) of the ABEE derivatives (I and II) purified by HPLC were subjected to 1D-$^{1}H$ NMR analysis. Whole spectra (a) and partial spectra of the acetyl proton region (b) of both derivatives are shown. Note that three and four major signals are detected in the acetyl proton region of derivatives I and II, respectively.

Fig. 5. Matrix-assisted laser desorption/ionization-time of flight mass spectrometry spectra derivatives I (a) and II (b). Spectra were acquired using a DHB matrix solution in reflectron mode (positive). Possible ions for major signals are indicated.

Fig. 6. Edited heteronuclear single quantum coherence spectroscopy (a) and heteronuclear multiple bond correlation (b) spectra of derivative I. The solution (approximately 5 mg/mL) of derivative I was subjected to analysis using 3-(trimethylsilyl)propionic acid and acetone as internal standards. Positive and negative heteronuclear single quantum coherence spectroscopy signals are indicated by red and green contour lines, respectively. The crosspeaks identified are designated as dC1 (correlation between C1 and H1 of unsaturated residue **C**), etc. The heteronuclear multiple bond correlation signals within the carbonyl carbon (C=O) region are displayed separately. The crosspeaks identified are designated as C=O/E(OAc) (correlation between C=O and *O*-acetyl protons of residue **E**), etc.

Fig. 7. Chemical structures of derivative I (a), derivative II (b), the sheath-forming polymer of *S. montanus* (c), and the sheath-forming polymer of *S. natans* (d). The arrows indicate the linkage cleaved by thiopeptidoglycan lyase.

Fig. 8 Comparative phase-contrast (left), epifluorescent (middle), and merged (right) images of immunostained filaments of *N*-biotinylated *S. montanus*. *S. montanus* was *N*-biotinylated and then cultivated. The bacterial filaments were recovered at 0 h (a) and 3 h (b) of cultivation and immunostained for visualization of the sheath. The edges of the sheath are not closed (a). A cultured (3 h) filament exhibited fluorescence only in the middle region (b).

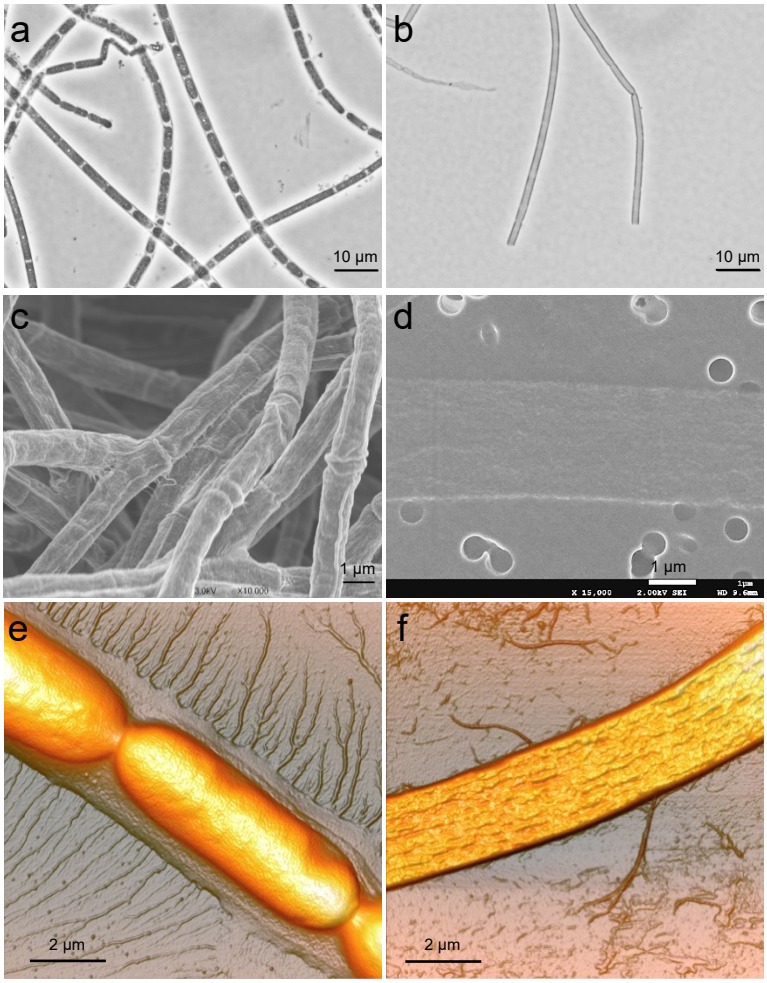


Fig. 1 - Takeda - *International Journal of Biological Macromolecules*

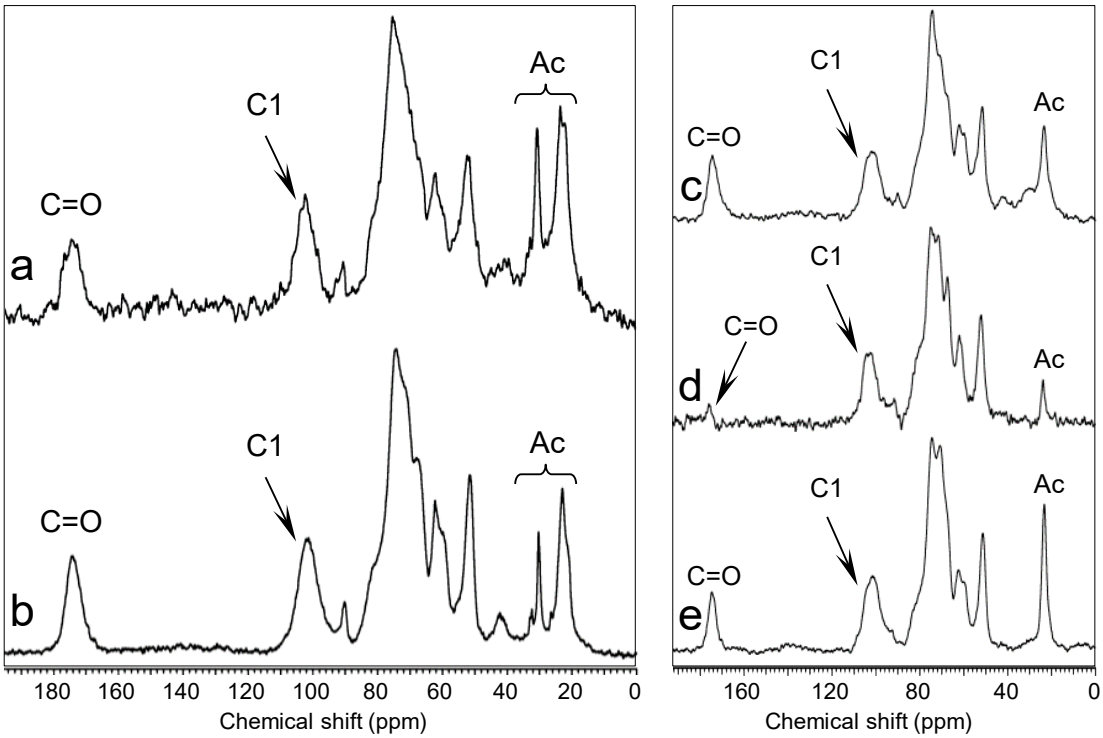


Fig. 2 - Takeda - *International Journal of Biological Macromolecules*

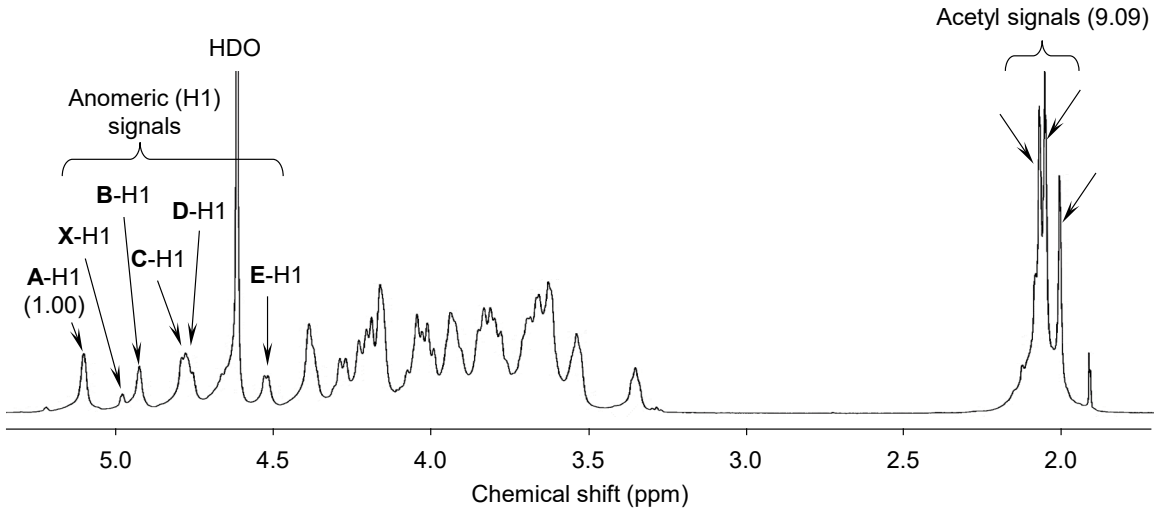


Fig. 3 - Takeda - *International Journal of Biological Macromolecules*

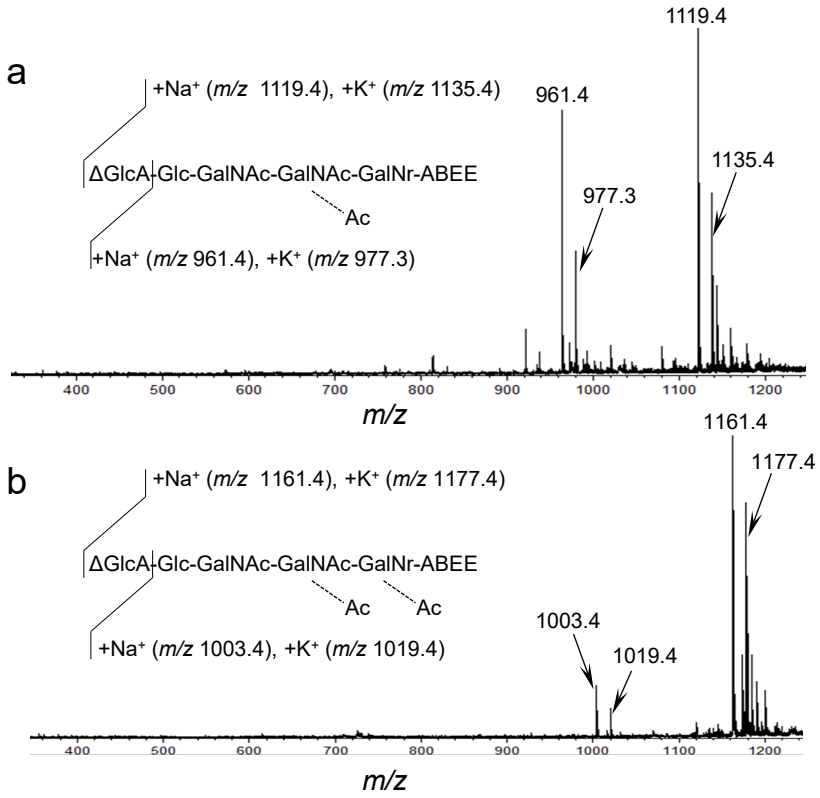


Fig. 4 - Takeda - *International Journal of Biological Macromolecules*

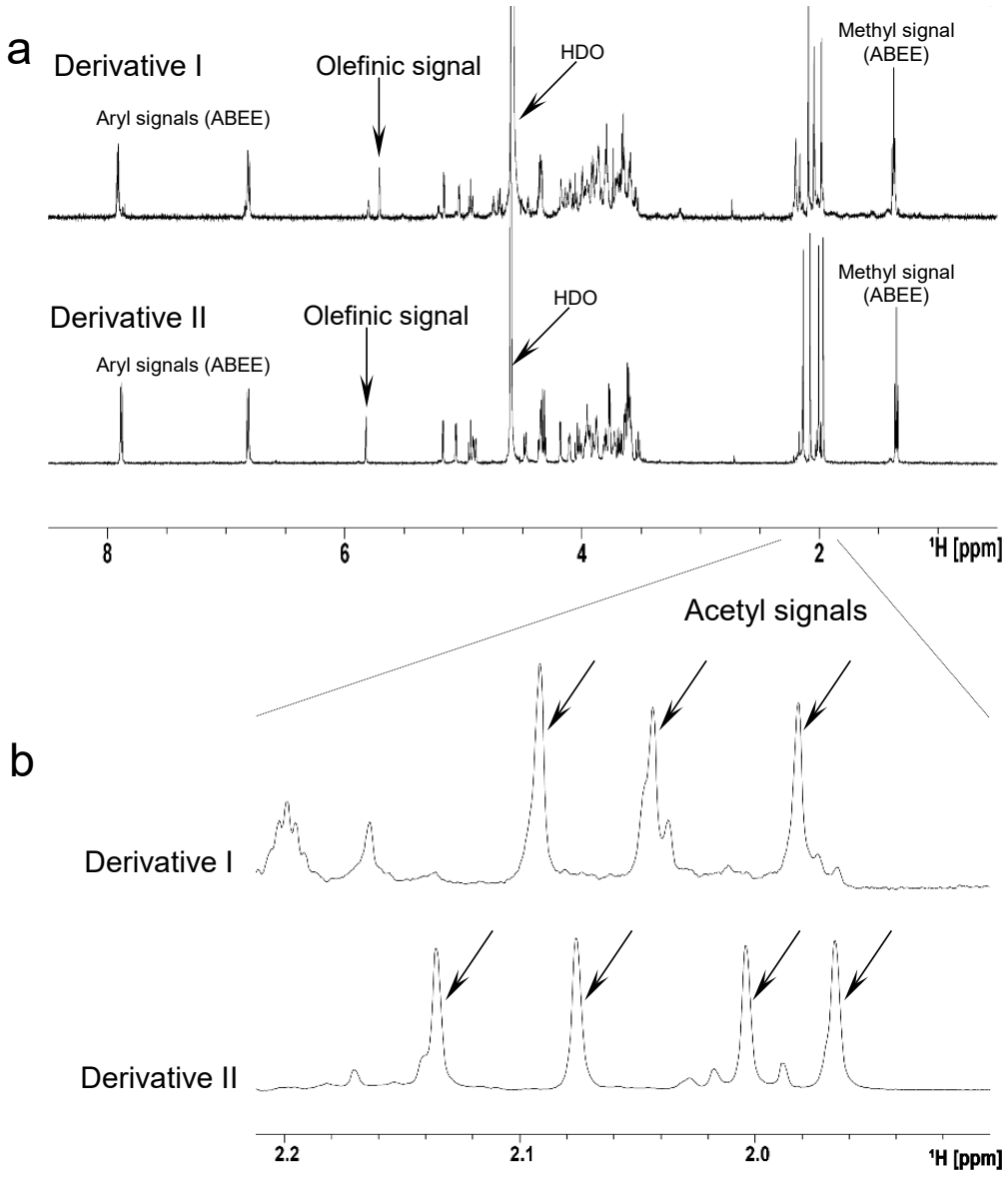


Fig. 5 - Takeda - *International Journal of Biological Macromolecules*

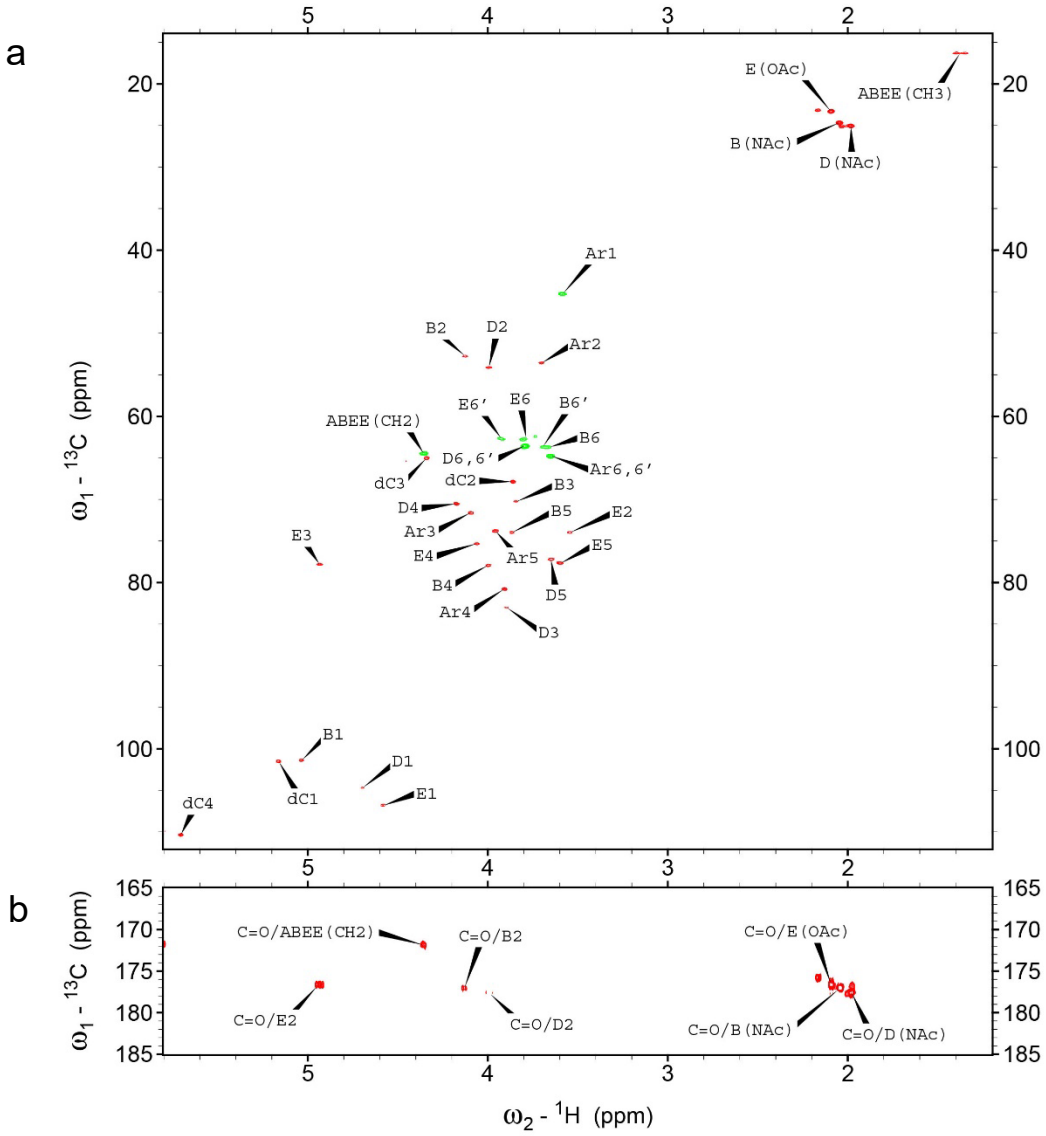


Fig. 6 - Takeda - *International Journal of Biological Macromolecules*

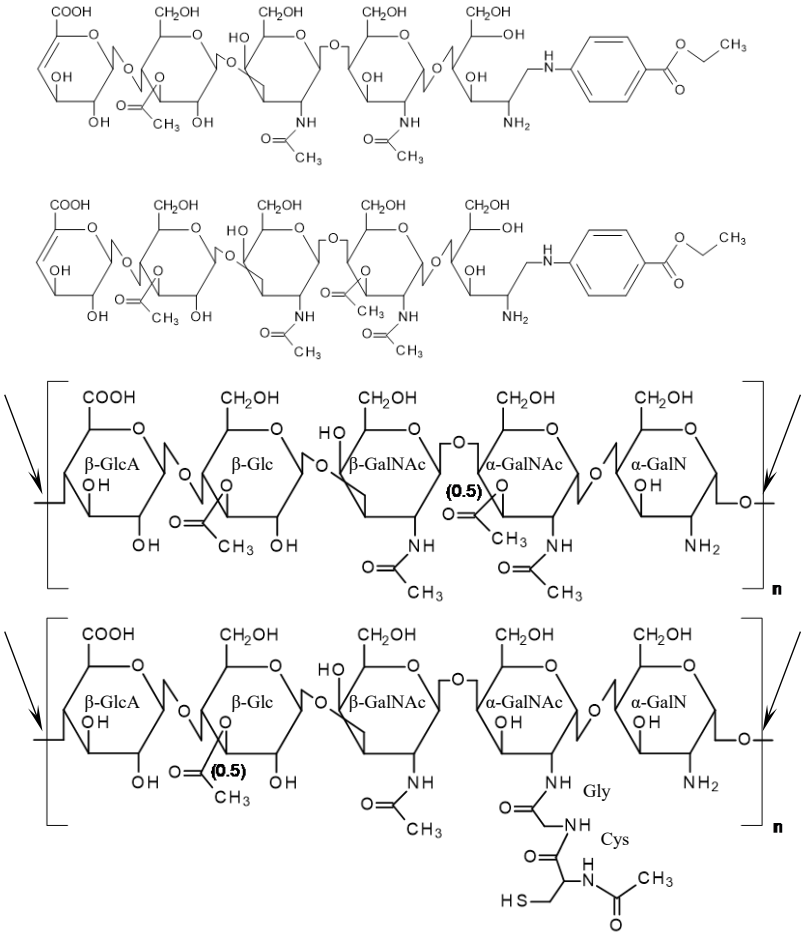


Fig. 7 - Takeda - *International Journal of Biological Macromolecules*

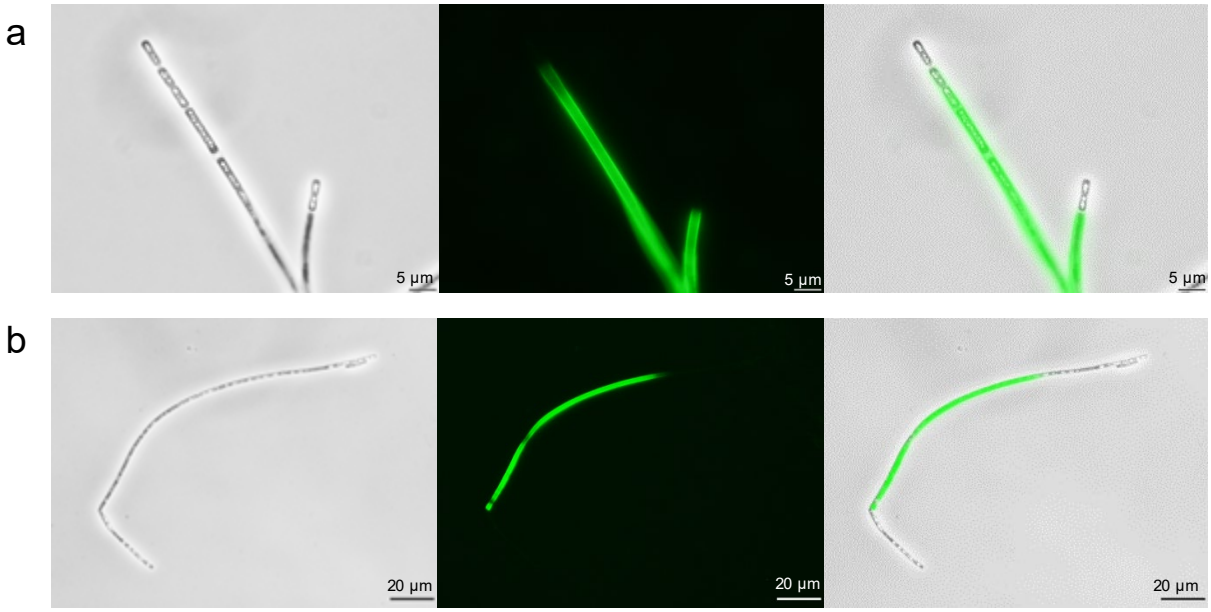


Fig. 8 - Takeda - *International Journal of Biological Macromolecules*